



Article

Rapid Fabrication of Homogeneous Submicron Silver Particles via a Microfluidic Chip and Use as a SERS Detection Substrate

Junjie Chen ^{1,†}, Suyang Li ^{2,†}, Fuqi Yao ¹, Wanbing Xu ², Yunfeng Li ³ , Qiang Chen ^{1,*} and Pei Liang ^{2,*} ¹ College of Metrology and Measurement Engineering, China Jiliang University, Hangzhou 310018, China² College of Optical and Electronic Technology, China Jiliang University, Hangzhou 310018, China³ College of Information Engineering, China Jiliang University, Hangzhou 310018, China

* Correspondence: chenqiang_cjlu@cjlu.edu.cn (Q.C.); plianghust@cjlu.edu.cn (P.L.)

† These authors contributed equally to this work.

Abstract: Silver particles have been widely used in SERS detection as an enhancement substrate. The large-scale synthesis of Ag particles with controllable size and shape is still a challenge. We demonstrate a high-throughput method for the preparation of monodisperse submicron silver particles using S-shaped microfluidic chips. Submicron silver particles were prepared by a simplified reduction method. By adjusting the concentration of the reducing agent ascorbic acid and the stabilizer PVP, the particle size and morphology could be controlled, obtaining a size distribution of 1–1.2 μm for flower-like silver particles and a size distribution of 0.5–0.7 μm for quasi-spherical silver particles. This microfluidic system can be used to fabricate submicron silver particles on a large scale, continuously and stably, with a production efficiency of around 1.73 mg/min. The synthesized submicron silver particles could realize ultra-sensitive SERS detection, and the lowest concentration of rhodamine 6G (R6G) that could be detected was 10^{-9} M.

Keywords: submicron silver particles; microfluidic chip; SERS detection



Citation: Chen, J.; Li, S.; Yao, F.; Xu, W.; Li, Y.; Chen, Q.; Liang, P. Rapid Fabrication of Homogeneous Submicron Silver Particles via a Microfluidic Chip and Use as a SERS Detection Substrate. *Chemosensors* **2023**, *11*, 232. <https://doi.org/10.3390/chemosensors11040232>

Academic Editor: Barbara Palys

Received: 3 February 2023

Revised: 31 March 2023

Accepted: 6 April 2023

Published: 7 April 2023



Copyright: © 2023 by the authors. Licensee MDPI, Basel, Switzerland. This article is an open access article distributed under the terms and conditions of the Creative Commons Attribution (CC BY) license (<https://creativecommons.org/licenses/by/4.0/>).

1. Introduction

Silver nanoparticles (AgNPs) have been widely used in the fields of medicine [1], energy [2], electronics [3], materials [4], and catalysis [5], due to their excellent electrical conductivity, thermal conductivity, antibacterial properties, and catalytic properties [6–12]. They are also used in biomarking, water treatment, drug delivery, cancer treatment, as antibacterial agents, and in surface coating [13–18]. Silver nanoparticles also demonstrated an excellent surface plasmon resonance (SPR) effect [19], which has sparked interest in their use as sensors, biological labels, and substrates for surface-enhanced Raman scattering (SERS). Silver nanoparticles after surface roughening exhibit high SERS activity and are widely used as efficient SERS substrates [20]. The efficiency of the SERS signal depends heavily on the geometrical characteristics and the surface roughness of the metallic nanostructure [21]. Small variations in either geometrical characteristics or surface roughness of the metal nanostructure provoke huge fluctuations in SERS intensity. Those SERS intensity variations cause large uncertainties in analytical calibration, large variability between measurements, and unreliable determinations. The transition of SERS to analytical applications requires good reproducibility and repeatability; however, the low reproducibility has hindered the widespread use of SERS in analytical chemistry. Therefore, controlling the particle morphology and size distribution is crucial to expanding SERS assay applications.

In the past decades, many synthetic methods have been proposed to fabricate AgNPs [22,23]. The preparation methods of metal nanoparticles can be divided into two main categories [24]: (1) physical methods, such as evaporation/condensation [25] or laser ablation [26], which require the use of professional instruments and high energy to increase the reaction temperature and thus usually generate high costs and require a long reaction time [27]; (2) chemical methods [18,28,29], during which the metal ions in the solution are reduced. The silver

ions in AgNO_3 or AgClO_4 salts are reduced by the reducing agent, and then these reduced silver atoms agglomerate to form metallic silver nuclei, which gradually form nanoparticles. The chemical reduction method has the advantage of saving time and money [30]. However, both of these two synthesis methods have certain disadvantages, especially for rapid reactions, since, due to the inability to control heat and mass transport rapidly, it is difficult to achieve a precise shape control of the nanoparticles, which limits the progress of nanotechnology and the resulting economic benefits [31–34]. As the application of nanoparticles becomes more and more widespread and systematic, it is urgent to achieve a high yield in the near future.

Due to uniform flow, uniform mixing, easy control, high efficiency, continuous operation, and low cost, the preparation technology of microfluidic particles has developed rapidly [35–38]. The microfluidic reactor is an excellent tool for synthesizing a variety of nanoparticles and can allow the precise control of the particle size, particle size distribution, and batch-to-batch reproducibility [39–41]. The microfluidic chip strengthens the mass transfer and heat transfer rate in a micron-level restricted environment, which can accurately control the particle morphology. It can reduce the particle size of the nanoparticles while ensuring their uniformity, providing more advantages compared with traditional methods [42]. Microfluidic chips have unique fluid properties in a micro-scale environment, which can provide excellent mixing efficiency and a feasible route for the synthesis of noble metal nanoparticles. Microfluidic synthesis can produce micro- or nano-sized particles with narrow size distribution and consistent morphology by a proper flow rate and appropriate mixing [43–46]. The automated microfluidic synthesis system driven by a continuous liquid phase pump can be used as a specific synthesis environment for the high-throughput synthesis of various nanostructures of semiconductor or metal materials, such as nanospheres, nanorods, and even nanosheets [47,48]. In addition, benefiting from the closed nature of the microfluidic chip itself, the reaction solution in the chip can effectively avoid the interference of the external environment, which can greatly improve the repeatability of the experimental results [49–52]. For example, Xu et al. [53] used a microfluidic droplet flow to enhance the mass transfer performance of liquid–liquid systems and prepared Ag nanoparticles by reducing metal salt aqueous solutions. The effects of different experimental conditions on the diameter, shape, particle size distribution, and elemental composition of silver particles were investigated, and the smallest diameter of the synthesized nanoparticles was less than 5 nm. Magdalene et al. [54] improved the mixing efficiency by using a Y-shaped serpentine micromixer and studied the method of green synthesis of silver nanoparticles using extracts of traditional medicinal plants. The synthesized silver nanoparticles had a small size (~80 nm) and a strong antibacterial effect. This microfluidic preparation effectively reduces the necessary sample amount of important medicinal plants and the time required for the synthesis of the nanoparticles and provides space for the development of green lab-on-a-chip devices. Liu et al. [55] proposed a new synthesis method to prepare AgNPs, which uses a piezoelectric-actuated three-phase flow-pulsating mixing microfluidic chip. Compared with other synthesis methods, the synthesis of AgNPs by this microfluidic chip is fast, simple, and controllable. The average particle size of the synthesized spherical silver nanoparticles was about 29 nm, with high yield, uniform morphology, and good dispersibility.

In this work, we used silver nitrate (AgNO_3) as a precursor, PVP as a stabilizer, and ascorbic acid as the reducing agent to prepare submicron silver particles with high throughput on an S-type microfluidic chip. This method is simple to operate, inexpensive, and fast. This method allows the preparation of silver particles with different particle sizes and morphologies. As a green and environmentally friendly material, ascorbic acid does not produce heavy metals or organic pollution. The concentration of PVP and ascorbic acid are important parameters to control the morphology and size distribution of the particles. By adjusting these two parameters, silver particles with two different structures were successfully prepared. Scanning electron microscopy and transmission electron microscopy were used to characterize the morphology and size of the particles.

The SERS detection results showed that the SERS substrate made from the synthesized submicron silver particles has excellent SERS activity, and the SERS signal of R6G could still be detected at a concentration of only 10^{-9} M.

2. Methodology and Characterizations

2.1. Materials

The materials for the chip fabrication in this paper consisted of the SU8-3025 negative photoresist (MicroChem, Newton, MA, USA), Sylgard 184 polydimethylsiloxane (PDMS, Dow Corning, Midland, MI, USA), and microscopic slides (Feizhou Corp, Yancheng, China). Silver nitrate (AgNO_3 , >99%) and ascorbic acid ($\text{C}_6\text{H}_8\text{O}_6$, >99%) were purchased from Aladdin Chemical Reagent Co., Ltd. (Shanghai, China). Polyvinylpyrrolidone (PVP, MF: $\text{C}_6\text{H}_9\text{NO}$), rhodamine 6G (R6G, >99%), and nitrofurantoin ($\text{C}_8\text{H}_6\text{N}_4\text{O}_5$, >99%) were obtained from Macklin reagent Inc. (Shanghai, China).

2.2. Instruments

The microchip was fabricated using a UV lithography machine (URE-2000/25, Institute of Optics and Electronics, Chinese Academy of Sciences). The PDMS chip was irreversibly bonded to a glass slide using oxygen plasma treatment (PDC-32G-2, HARRICK). The solutions were infused into the microfluidic chip using syringe pumps (Pump 11 Elite, Harvard Apparatus). The structure of the silver particles was characterized by a scanning electron microscope (SEM, HITACHI SU8010, resolution: 1.0 nm). The composition of the particles was analyzed by energy-dispersive spectroscopy (EDS, Apollo XL, EDAX, energy resolution: 129 eV). The transmission electron microscopy (TEM) images were obtained using FE-TEM (Tecnai TF30 ST). The optical absorption spectra were measured using a UV-Vis spectrophotometer (TU-1901, PERSEE). The SERS spectra of the probe molecules were measured with a confocal microscope/Raman spectrometer system (Horiba, LabRAM HR).

2.3. Microfluidic Devices

Fabrication of the microfluidic chip. The microfluidic chip included two parts: a PDMS microchannel and a glass substrate. The specific production method was as follows, and the specific production process is shown in Supplementary Information Figure S1.

To fabricate parts of the PDMS microchannel, a photomask was first designed and fabricated, and then a SU-8 master mold was fabricated on a silicon wafer using standard photolithography. In this step, the silicon wafers were coated twice at 1000 rpm with the SU8-3025 negative photoresist to obtain a large microchannel depth, and the wafers were soft-baked on the hot plate at 65°C for 1 h after the first coating and before the second coating, to increase the adhesion of the two layers during the second coating. The time of UV lithography was 19 s, and the exposure energy was $15\text{ mW}/\text{cm}^2$. Then, the degassed PDMS prepolymer, in which the ratio between the precursor and the cross-linking catalyst was 10:1, was cast on the master mold and placed on the hot plate for curing at 95°C for 1 h. After completing the previous steps, the cured PDMS microchannel chips were peeled from the master molds and cut to an appropriate size. The inlet and outlet of the microchannel were created using a puncher on the PDMS chips. Last, the PDMS chips and the glass were bonded and placed in an oven at 65°C for 2 h to enhance the bonding, after they were treated with oxygen plasma for 3 min. Through the test of the chip section by a Step profiler, we determined that the depth of the microchannel was $120\ \mu\text{m}$, and the width was $300\ \mu\text{m}$.

2.4. Manufacturing Submicron Silver Particles by Microfluidics

Submicron silver particles were synthesized in a microfluidic chip by the chemical reduction method. Figure 1i shows a schematic diagram of the experimental setup. The overall design structure of the microfluidic chip is shown in Figure 2a. The size of the microfluidic chip was $28 \times 10\ \text{mm}^2$. The reactor consisted of three S-shaped channels and two circular chambers, which were designed to optimize the mixing efficiency of the

three-phase solution and prevent the backflow. The microfluidic chip had three inlets and one outlet. The inlet was connected to a syringe pump through three polyethylene tubes, and the outlet was connected to a test tube through a polyethylene tube. In the experiments, the flow rate of all solutions was 1 mL/min. The precursor AgNO_3 and the dispersant PVP were pumped into inlet A and inlet B, respectively. The two-phase solutions were fully mixed after passing through the S-shaped channel. The reducing agent ascorbic acid was pumped from inlet C and came in contact with the mixed solution of phases A and B in the main channel. The velocity flow fields of the three solutions in the designed microchannel are shown in Figure 2b. With the contact of the three-phase solution, the silver ions in the mixed solution of the phases A and B were reduced by ascorbic acid to silver atoms and grew into silver particles.

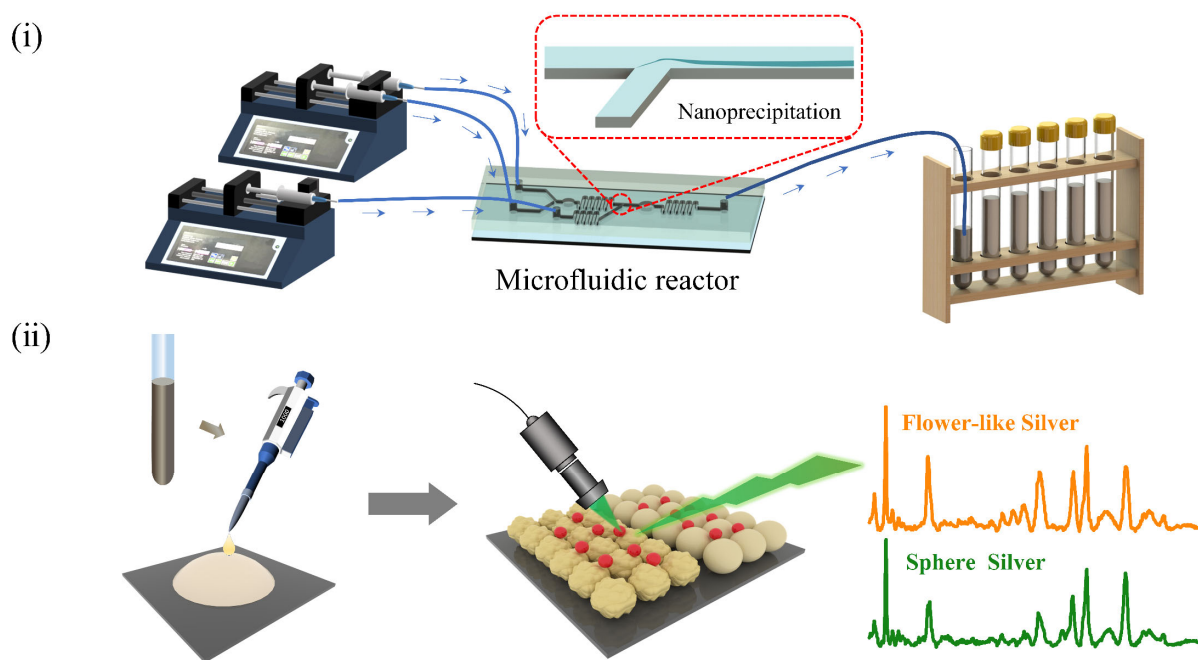


Figure 1. A schematic diagram of the device for fabricating submicron silver particles in a microfluidic chip and the synthesized silver particles that were used for SERS detection. (i) Microreactor part: the three-phase solution was pumped into the microchip for the reaction to occur and generate particles, collected in the test tube; (ii) SERS detection part: the synthesized particles were used as SERS substrates for SERS detection to evaluate their Raman enhancement effect.

Synthesis of flower-like silver particles via a microfluidic chip. AgNO_3 , PVP, and ascorbic acid were dissolved in deionized ultrapure water. The concentration of AgNO_3 was always 0.02 M, the concentration of PVP was 0.2% (wt%), and the concentration of ascorbic acid was 0.01 M. The three-phase solutions were passed into the microfluidic chip at a flow rate of 1 mL/min.

Synthesis of quasi-spherical silver particles via a microfluidic chip. AgNO_3 , PVP, and ascorbic acid were dissolved in deionized ultrapure water. The concentration of AgNO_3 was kept unchanged at 0.02 M, the concentration of PVP was increased to 1% (wt%), and the concentration of ascorbic acid was adjusted to 0.1 M. Similarly, the three-phase solutions were passed into the microfluidic chip at a flow rate of 1 mL/min.

Synthesis of quasi-spherical silver particles via conventional equipment. We stirred 10 mL of AgNO_3 solution (0.02 M) and 10 mL of PVP solution (1%) in a magnetic stirrer at room temperature. Then, 10 mL of ascorbic acid solution (0.1 M) was quickly added into the above mixed solution and stirred for 15 min.

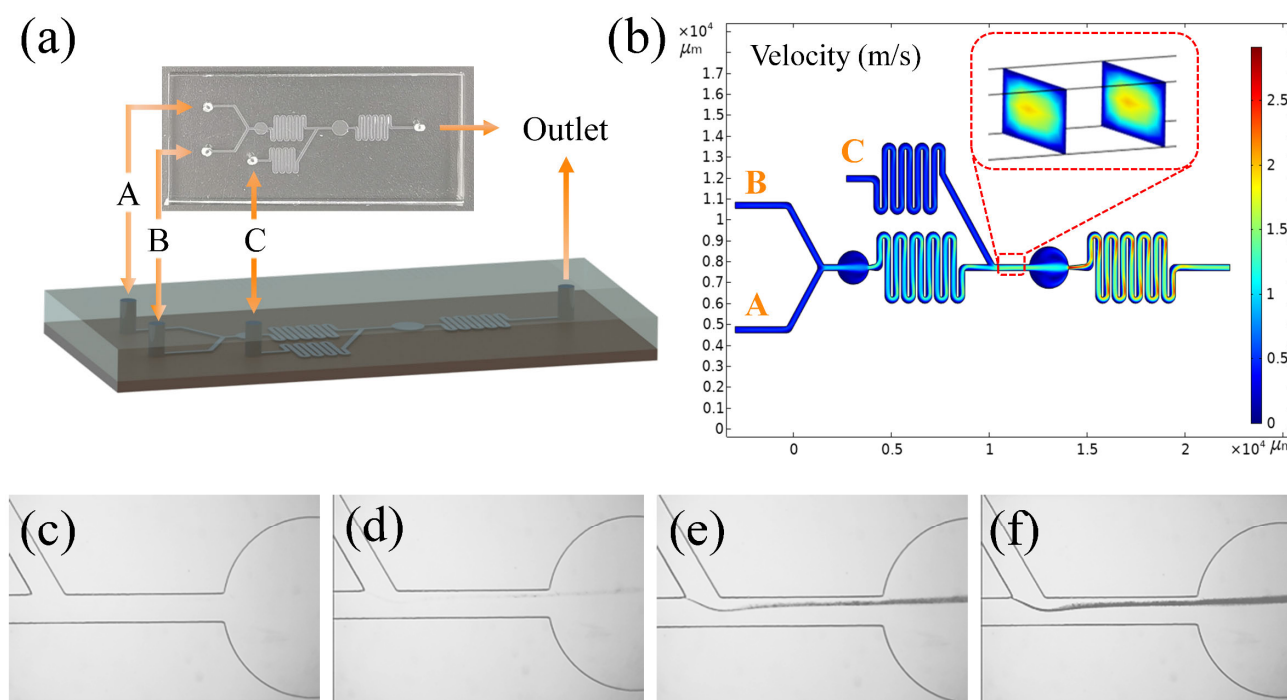


Figure 2. Synthesis of silver particles in microchannels. (a) Design structure diagram of the microchannel and physical diagram of the chip; (b) a simulation software was used to simulate the flow rate of the solution in the microchannel; the magnified portion is the channel cross-sectional flow rate distribution after the contact of the three-phase solution; (c–f) change of the laminar contact surface with time ((c–f): 0 s, 4 s, 20 s, 60 s): the reduction reaction occurred on the laminar contact surface to generate particles and continued to occur as time increased, causing the accumulation of the particles and producing color changes.

2.5. SERS Measurement

The preparation of the silver particles as a SERS substrate and SERS detection are shown in Figure 1ii. As indicated, 20 μL of silver particles solution was dropped on a $5 \times 5 \text{ mm}^2$ silicon wafer, and then the silicon wafer was transferred to a vacuum oven and dried at 45 $^\circ\text{C}$ for 6 h.

SERS measurement. R6G with a concentration gradient of 10^{-9} M – 10^{-4} M and a nitrofurantoin antibiotic solution of 10^{-8} M – 10^{-3} M were prepared for SERS detection. About 30 μL of the sample solution was dropped onto the prepared SERS substrate, and then the substrate was evaporated naturally by placing it at room temperature for about 5 h. The Raman spectra were obtained using an excitation wavelength of 633 nm and a range of 550–1800 cm^{-1} . Five different points were selected on each SERS substrate. The Raman mapping was obtained by integrating the intensity of the Raman band at 613 cm^{-1} with a measurement range of $50 \times 50 \mu\text{m}^2$ and a step size of 2 μm .

3. Results and Discussion

3.1. Reduction Reaction in Microchips

When the three-phase solution was pumped into the microchip at a flow rate of 1 mL/min, according to the Reynolds number $\text{Re} = \rho v d / \mu$, Re was less than the critical value Re_c (about 2300–2800), and the mixed solution presented a laminar flow in the microchannel [56]. As shown in Figure 2b, the flow velocity of the fluid was maximum in the center of the channel and minimum near its walls. On the contact surface of the laminar flow, the reduction reaction occurred in the three-phase solution, particles were generated, and a small number of particles accumulated on the wall. Figure 2c–f shows that as the reaction continued, the color of the contact surface on the laminar flow contact surface of the through channel gradually darkened due to the gradual accumulation of particles, but

this accumulation never spread to the wall surface of the channel. When the three-phase mixed solution left the straight channel and entered the S-shaped channel, the fluid velocity on both sides of its near wall changed due to the difference in curvature at the bend, the fluid flow velocity on the outer wall side became smaller, and the flow velocity on the inner wall side became larger; this phenomenon was reversed at the next bend. After several S-shaped bends, the laminar flow state of the fluid was disturbed, the mixing efficiency was improved, and the reduction reaction gradually spread throughout the channel. The design of an S-shaped channel not only improved the mixing efficiency but also increased the reaction time per unit area and improved the overall synthesis efficiency. While the S-shaped channel exhibited an excellent mixing efficiency, it also presented another problem, that is, a large number of particles accumulated on the surface of the channel. This phenomenon created a large particle waste, and we are still researching this phenomenon, hoping to find a good way to solve the problem of particles building up on the walls.

3.2. Characterization of Submicron Silver Particles

A sample of the silver particles was obtained by centrifugation and washed with ethanol several times to remove the excess surfactant. The morphology of the synthesized particles was investigated by SEM, and typical particle images are shown in Figure 3a,b. These particles had spherical profiles but highly rough surfaces consisting of many irregular and randomly arranged protrusions. The SEM images showed that we successfully synthesized flower-like silver particles with a highly rough surface and a diameter of about 2000 nm. Their crystal structure and phase composition were characterized by an X-ray diffractometer (XRD). Figure 3e shows a typical X-ray diffraction pattern of the as-synthesized silver particles. Three diffraction peaks were observed, which corresponded to the diffraction peaks of the (111), (200), and (220) planes. The elemental composition of the particles was analyzed by EDS. Figure S2a–c shows typical EDS spectra of individual flower-like particles. A strong main emission peak of silver is observed in Figure S2c, thus emphasizing that the synthesized particles were composed of Ag elements. In addition, since the characterization of the particles was performed on silicon wafers, a small Si signal also appeared. No further impurities were observed in the EDS spectrum.

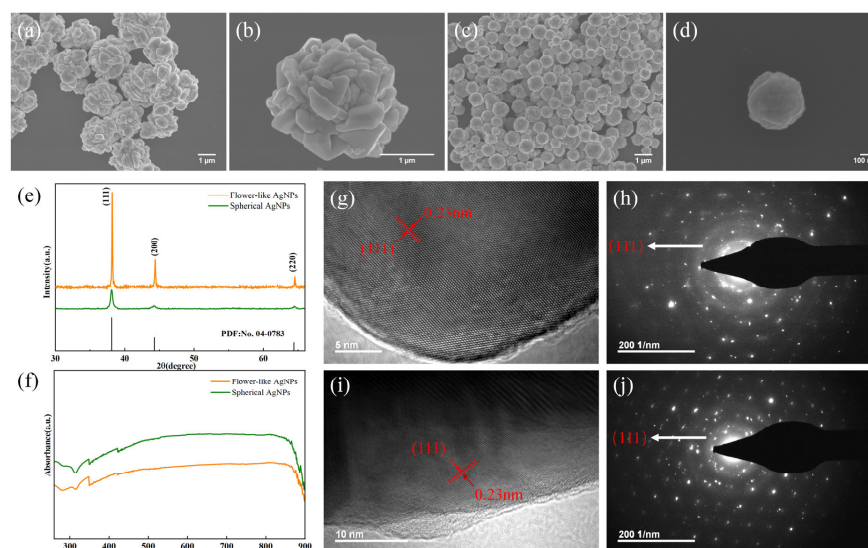


Figure 3. Characterization of silver particles synthesized under different synthesis conditions. (a,b) SEM images of the synthesized flower-like silver particles and their detailed morphology; (c,d) SEM images of the synthesized quasi-spherical silver particles and their detailed morphology; (e) typical XRD spectrum of silver particles; (f) UV–Vis absorption spectra of the flower-like silver particles and quasi-spherical silver particles; (g,h) HR-TEM and electron diffraction pattern of a selected area of the flower-like silver particles; (i,j) HR-TEM and electron diffraction pattern of a selected area of the quasi-spherical silver particles.

When the concentration of a solution changes, the morphology of the particles also changes. In the experiment, changes in particle morphology were observed by changing the concentration of ascorbic acid and PVP. Under the conditions of keeping the concentration of AgNO_3 unchanged and using a concentration of ascorbic acid of 0.1 M and a concentration of PVP of 1%, quasi-spherical silver particles with a size of 600 nm were obtained. Likewise, the micro-morphology of the particles was obtained by SEM, and XRD and EDS were used to verify the elemental composition of the particles. Figure 3c,d shows the SEM images of the synthesized large-scale quasi-spherical silver particles and their detailed morphology. Figure S2d–f shows the EDS spectrum of the quasi-spherical silver particles, which proved that the particles were composed of silver element. It can be seen from the SEM images that the surface of the quasi-spherical silver particles was smooth, and the particle size was greatly reduced compared with that of the flower-like silver particles. We measured the size of 100 particles randomly selected and found that the average particle size of the quasi-spherical silver particles was about 598 nm, and the relative standard deviation (RSD) of the particle size was 14.2%.

The modes of surface plasmon resonance excitation in metal particles with different morphology and size are different, so the absorption peaks caused by SPR in the UV–Vis absorption spectra are also different. As shown in Figure 3f, silver particles with two morphologies showed an absorption peak around 420 nm, which was attributed to the surface plasmon resonance. The absorption peak of the flower-like silver particles was slightly red-shifted relative to that of the quasi-spherical silver particles, indicating that the flower-shaped silver particles had a relatively large particle size. The silver particles with the two morphologies showed the same weak absorption near 350 nm, which was the plasmon resonance absorption peak with partial block or sheet metal Ag in the solution.

Figure 3g,h shows the lattice streaks and electron diffraction (SAED) maps of a selected area of the flower-like silver particles. Likewise, Figure 3i,j show the lattice streaks and SAED maps of the quasi-spherical silver particles. Multiple equally spaced lattice fringes could be observed by high-resolution TEM. The lattice spacing (d) of the (111) plane was found to be 0.23 nm, consistent with the JCPDS data (No.04-0783). The SAED pattern showed circular fringes, in agreement with the XRD data (Figure 3e). These results further confirmed the formation of silver particles with a highly crystalline nature, and the stronger XRD peak indicated that the crystallinity of the flower-like particles was higher than that of the quasi-spherical silver particles.

3.3. Factors Affecting the Morphology of the Silver Particles

The process of synthesizing silver particles in a microreactor can be divided into three stages, namely, the reduction stage, the nucleation stage, and the growth stage. During the reaction process, the stabilizer PVP will preferentially adhere to a certain crystal surface of the nanocrystalline nucleus, causing the free energy of the crystal surface to change, reducing the growth rate of these crystal surfaces, and leading to anisotropic growth of the crystal, which results in different structures [57–59]. PVP was also used as a stabilizer to prevent the aggregation of the silver particles [60]. Aggregation is due to the high surface energy and thermodynamic instability exhibited on the surface of the particles. Stabilizers or surfactants help to reduce the surface tension of a liquid and make the particles more easily dispersed in it. On the other hand, the use of a reducing agent can also induce modifications of the particle morphology. The concentration of the reducing agent ascorbic acid will affect the concentration of silver atoms in the reduction stage, resulting in a change in the number of silver nuclei in the nucleation stage, which will affect the final morphology.

In the above experiments, silver particles of different morphology were obtained by changing the concentration of PVP and ascorbic acid. The two types of silver particles with different morphologies indicated that the concentration of ascorbic acid and PVP had an important effect on the morphology of the synthesized silver particles. When the concentration of ascorbic acid increased from 0.01 M to 0.1 M, the concentration of the reducing agent in the reaction system increased greatly. A higher concentration of

the reducing agent could accelerate the reduction rate and increase the concentration of silver atoms in the reaction system. The increase in silver atom concentration sped up the nucleation rate, making the nucleation rate of the silver particles higher than their growth rate, and the concentration of the silver nuclei increased. The increasing concentration of the silver nuclei led to the formation of a large number of small particles in the solution, which made it easier to synthesize uniform small-size silver particles. On the other hand, the concentration of the stabilizer also affected the particle size. Generally, the larger the ratio of water to the stabilizer, the larger the particle size of the synthesized particles. When the PVP concentration was increased from 0.2% to 1%, the ratio of water to stabilizer decreased, resulting in a large reduction in the particle size. In addition, the high concentration of PVP also increased the coverage of the silver core. In this case, the number of exposed crystal faces was relatively small, which led to a nearly isotropic growth rate of the crystal nuclei. The surface roughness of the silver particles was significantly reduced, and the particles tended to be more spherical.

3.4. Comparison of Silver Particles Prepared by the Microfluidic Chip and the Conventional Method

We compared the size distribution obtained in the microreactor with that obtained by conventional synthesis equipment. A reference experiment was performed twice using the synthesis conditions of the quasi-spherical silver particles in a beaker to ensure repeatability. The resulting sample is shown in Figure S3. By comparison, it was found that the particles synthesized by conventional equipment had a fairly wide size distribution. To quantitatively analyze the above synthetic result, we measured the size of 100 particles, randomly chosen in Figure S3a. The size of the particles was determined by measuring the longest length of the particles, and the particle size distribution histogram comparison is shown in Figure S4. The average size of the silver particles was 515 nm, and the decrease in particle size was caused by the uneven distribution of the particle size. Compared with microfluidic synthesis, the RSD of the size of the silver particles synthesized by the conventional device reached 29.1%, showing an increase of 14.9%. The results proved that under similar experimental conditions, the microfluidic synthesis of particles provided advantages, and particles with a more uniform particle sizes could be synthesized.

3.5. SERS Enhancement Effect

Before SERS detection, to ensure that the silver substrate did not interfere with the signal of the substance to be tested, SERS detection was conducted on a blank silver substrate, and the result showed that no interference signal appeared on the silver substrate (Figure S5). The SERS performance of two kinds of silver particles with different structures was evaluated by applying R6G as a probe molecule. The SERS activity of silver structures with different morphologies is shown in Figure 4a,d. As shown in the figures, in the SERS spectrum within the range of 550–1800 cm^{-1} , there were obvious peaks at 613 cm^{-1} , 773 cm^{-1} , 1363 cm^{-1} , 1511 cm^{-1} , and 1650 cm^{-1} , in agreement with previous work (the band assignments of the Raman peaks at different positions are shown in Table S1). The two kinds of silver particles synthesized by the microfluidic chip showed a very high SERS activity, and 10^{-9} M R6G could be detected. The Raman spectra of the silver structures clearly showed that the Raman intensities of R6G decreased as the concentration decreased (Figure 4a,c). For the sake of observation, the Raman intensities at a concentration from 10^{-7} M to 10^{-9} M were multiplied by an appropriate factor. The Raman characteristic peak at 613 cm^{-1} of R6G belongs to the in-plane bending mode of the carbon ring of xanthen. Taking the characteristic peak at this point as an example, the linear fitting of the intensities as a function of the concentration of R6G for the two different silver structures (Figure 4b,d), respectively, is shown in Equations (1) and (2):

$$Y = 31,523.4 + 4443.5 \log C \quad (1)$$

$$Y = 52,384.8 + 7314.5 \log C \quad (2)$$

where Y and C are intensity and concentration, respectively. The correlation coefficients R^2 of the flower-like silver particles and submicron silver particles were 0.969 and 0.967, respectively. The linear fitting results supported that the measured data were more accurate. The result showed that both silver structures had a low limit of detection and showed an excellent linear relationship. The enhancement factor (EF) of the prepared submicron silver particles under 633 nm laser is defined as:

$$EF = \frac{I_S \times C_R}{I_R \times C_S} \quad (3)$$

where I_S and I_R are the SERS intensity and normal Raman intensity of R6G at 613 cm^{-1} , respectively; C_S and C_R are the corresponding concentrations of R6G for SERS and normal Raman measurements, respectively. For the flower-like silver particles, the EF value was calculated as 3.95×10^5 , and for the quasi-spherical silver particles, EF was 6.22×10^5 .

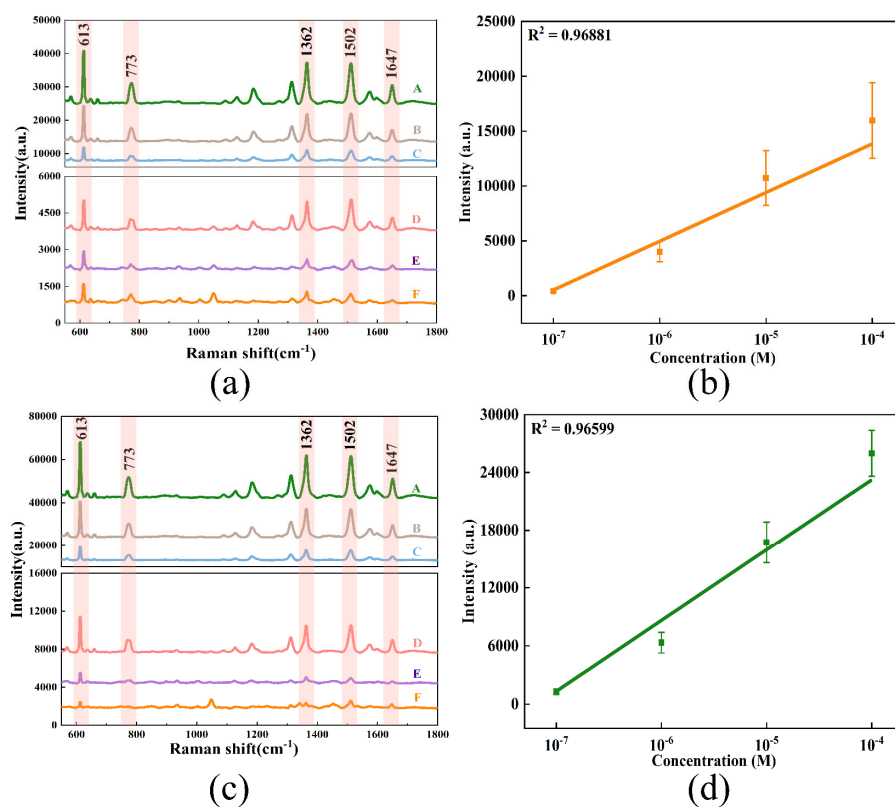


Figure 4. SERS spectra of R6G (A-F: 10^{-4} M– 10^{-9} M) adsorbed on the flower-like silver particles (a) and quasi-spherical silver particles (c) with the average intensity of the SERS signals; at 613 cm^{-1} as a function of the linear relationship of R6G concentration (b,d).

In order to study the reproducibility of the two silver structures and ensure the reliability of the data, the R6G probe molecule at a concentration of 10^{-6} M was dropped onto the substrate, and SERS was measured at more than 12 different locations, as shown in Figure S6a,d. The results showed that the relative standard deviations of SERS intensity at 613 cm^{-1} , 773 cm^{-1} , and 1363 cm^{-1} were 35%, 31%, and 37%, respectively. For the spherical silver nanostructures, the RSD of R6G were 14%, 11%, and 14%, respectively (Figure S4). The comparison results showed that the measurements of the quasi-spherical silver particles had a better reproducibility than those of the flower-like silver particles. The comparison results showed that the measurements of the quasi-spherical silver particles

had a better reproducibility than those of the flower-shaped silver particles. This was because the quasi-spherical silver particles had a relatively regular shape, and the LSPR intensity at each position was relatively consistent, with no significant fluctuation in the SERS enhancement effect, which could produce better a SERS signal repeatability. For the flower-like silver particles, because they had more irregular protrusions, the uneven distribution of hot spots in a region resulted in the irregular fluctuations of the SERS signals. At 613 cm^{-1} , a scale of 50×50 microns was selected for the Raman mapping test (Figure S6). Ignoring the error caused by intensity fluctuation and the distribution of the objects to be measured, the overall brightness of the image showed no significant difference, indicating a high uniformity of the entire substrate.

Nitrofurantoin is an effective antibiotic against bacterial infections and has been used in the past to combat conditions such as urinary tract infections [61]. However, it has been banned because it may produce toxic metabolites in animals. In order to study the sensitivity of the system for the trace detection of nitrofurantoin using the SERS effect based on silver structures, we used two kinds of silver substrates to detect nitrofurantoin and compared the differences in the Raman spectra (Figure 5a,c). The Raman peak at 1345 cm^{-1} was attributed to the vibration of $\omega(\text{H-C-H})$ VS ring, which was not easily interfered with by other peaks and could be used as the quantitative peak of nitrofurantoin. The peak position was used to linearly fit the peak strength and concentration (Figure 5b,d), using the linear Equations (4) and (5):

$$Y = 11,202.7 + 1567.6 \log C \quad (4)$$

$$Y = 12,655 + 1698.7 \log C \quad (5)$$

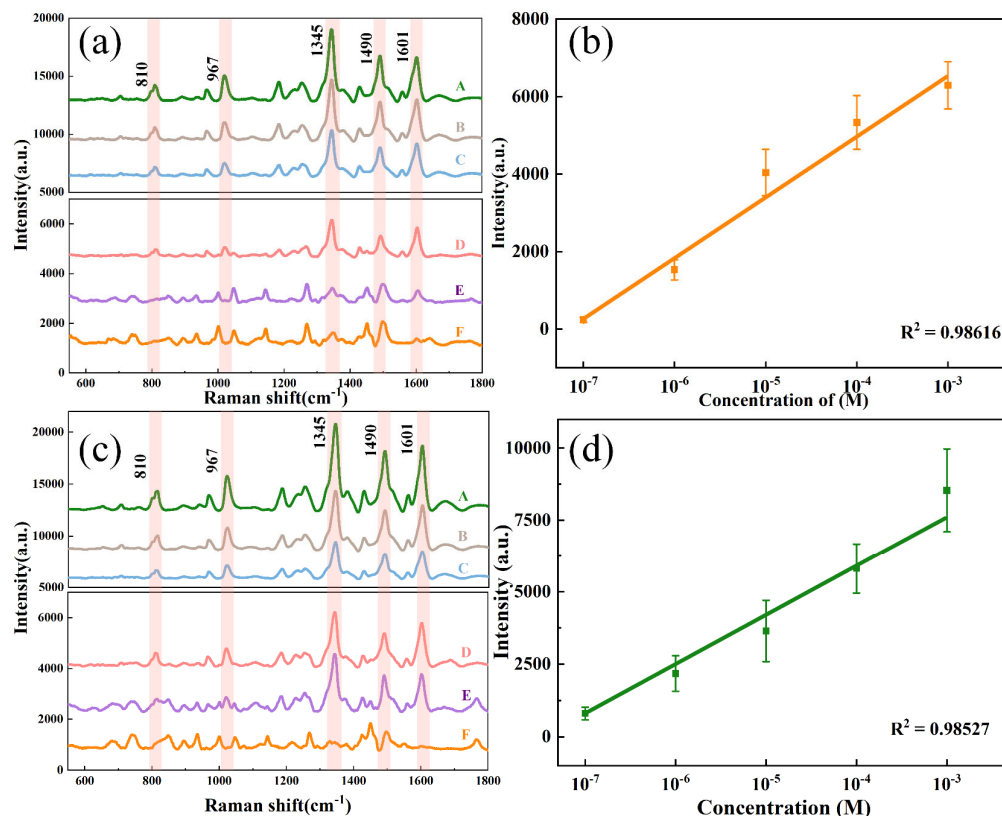


Figure 5. SERS spectrum of nitrofurantoin (A-F: 10^{-3} M – 10^{-8} M) on the flower-like silver particles (a) and quasi-spherical silver particles (c) and linear relationship between the SERS intensities at 1345 cm^{-1} and the concentration of nitrofurantoin (b,d).

The coefficients of determination (R^2) were 0.986 and 0.985, respectively. The above results showed that both silver structures could be used as effective SERS substrates for the accurate and sensitive SERS detection of actual samples.

4. Conclusions

In a word, we developed a simple and easy microfluidic system to synthesize two kinds of submicron silver particles with different particle sizes and morphologies, which could be used as SERS substrates for practical detection. The results showed that silver particles with uniform particle size can be prepared continuously and stably on a large scale in the microfluidic system. Based on a series of experiments, the possible growth mechanism of different silver particles was also explained. It was found that under the same precursor conditions, the concentration of reductant and stabilizer in the system can affect the number of nuclei and the coating degree of PVP on the nuclei, which has a great influence on the morphology and size of the particles. A SERS test showed that the two kinds of silver particles had high SERS activity, and the SERS signal could still be detected when the concentration of R6G was 10^{-9} M.

In addition, this work investigated the SERS spectra of nitrofurantoin based on the two kinds of silver particles. The results showed that the surface-enhanced Raman scattering signal could still be clearly observed when the concentration of nitrofurantoin was reduced to 10^{-8} M. The results showed that the synthesized silver particles can be used as an effective SERS substrate for trace detection and monitoring.

Supplementary Materials: The following supporting information can be downloaded at: <https://www.mdpi.com/article/10.3390/chemosensors11040232/s1>, Figure S1: Method for manufacturing PDMS chip; Figure S2: Typical EDS spectrum of flower-like silver particles (a–c) and quasi-spherical silver particles (d–f); Figure S3: Silver particles synthesized in conventional equipment; Figure S4: Particle size distribution histograms of particles prepared by microfluidic chips and conventional methods. (a) Particle size distribution histogram of the particles prepared by the microfluidic chip; (b) Particle size distribution histogram of particles prepared by traditional method; Figure S5: SERS blank control signals detected at five different positions when quasi-spherical silver particles were used as the SERS substrate; Figure S6: Reproducibility of flower-like silver particles (a–c) and quasi-spherical silver particles (d–f). (a,d): Silver particles with two morphologies were used as Raman substrates for signal intensities of SERS measurements at 12 different locations; (b,e): Relative standard deviation of SERS intensities for characteristic peaks at 613 cm^{-1} , 773 cm^{-1} , 1363 cm^{-1} ; (c,f): Raman mapping image of R6G (10^{-6} M) with all peak intensities at 613 cm^{-1} ; Table S1: Assignments of Raman bands of R6G in SERS and normal Raman conditions.

Author Contributions: Conceptualization, Q.C., P.L., J.C. and S.L.; methodology, J.C. and S.L.; software, J.C., F.Y. and W.X.; validation, J.C., S.L., F.Y. and Y.L.; formal analysis, J.C., S.L., Y.L., Q.C. and P.L.; investigation, F.Y., W.X. and Y.L.; resources, J.C., S.L., F.Y. and Y.L.; data curation, J.C., S.L. and F.Y.; writing—original draft preparation, J.C., S.L. and Q.C.; writing—review and editing, Q.C., P.L. and W.X.; visualization, W.X. and Y.L.; supervision, Q.C. and P.L.; project administration, Q.C. and P.L.; funding acquisition, Q.C., P.L. and Y.L. All authors have read and agreed to the published version of the manuscript.

Funding: This work was financially supported by the National Key R&D Program of China (No. 2018YFC0809100) and Beijing Science and technology project (No. Z201100009319001). The Project was financially supported by the National Key Research and Development Program project (No. 2017YFD040800) and the Zhejiang Provincial Natural Science Foundation of China (NO. LGF21F050002). The work was also greatly supported by the NMPA Key Laboratory for POCT Technology Transforming and Quality Control.

Institutional Review Board Statement: Not applicable.

Informed Consent Statement: Not applicable.

Data Availability Statement: Data sharing not applicable.

Conflicts of Interest: The authors declare no conflict of interest.

References

1. Chugh, H.; Sood, D.; Chandra, I.; Tomar, V.; Dhawan, G.; Chandra, R. Role of gold and silver nanoparticles in cancer nanomedicine. *Artif. Cells Nanomed. Biotechnol.* **2018**, *46*, 1210–1220. [[CrossRef](#)] [[PubMed](#)]
2. Pradeep, N.; Paramasivam, K.; Rajesh, T.; Purusothamanan, V.S.; Iyahraja, S. Silver nanoparticles for enhanced thermal energy storage of phase change materials. *Mater. Today-Proc.* **2021**, *45*, 607–611. [[CrossRef](#)]
3. Shankar, A.; Salcedo, E.; Berndt, A.; Choi, D.; Ryu, J.E. Pulsed light sintering of silver nanoparticles for large deformation of printed stretchable electronics. *Adv. Compos. Hybrid Mater.* **2017**, *1*, 193–198. [[CrossRef](#)]
4. Zhang, J.P.; Li, H.T.; Xu, T.; Wu, J.J.; Zhou, S.L.; Hang, Z.H.; Zhang, X.H.; Yang, Z.H. Homogeneous silver nanoparticles decorating 3D carbon nanotube sponges as flexible high-performance electromagnetic shielding composite materials. *Carbon* **2020**, *165*, 404–411. [[CrossRef](#)]
5. Qi, L.B.; Zhang, K.M.; Qin, W.; Hu, Y.X. Highly efficient flow-through catalytic reduction of methylene blue using silver nanoparticles functionalized cotton. *Chem. Eng. J.* **2020**, *388*, 124252. [[CrossRef](#)]
6. Vega-Baudrit, J.; Gamboa, S.M.; Rojas, E.R.; Martinez, V.V. Synthesis and characterization of silver nanoparticles and their application as an antibacterial agent. *Int. J. Biosens. Bioelectron.* **2019**, *5*, 166–173. [[CrossRef](#)]
7. Panacek, A.; Kolar, M.; Vecerova, R.; Prucek, R.; Soukupova, J.; Krystof, V.; Hamal, P.; Zboril, R.; Kvittek, L. Antifungal activity of silver nanoparticles against *Candida* spp. *Biomaterials* **2009**, *30*, 6333–6340. [[CrossRef](#)]
8. Morones, J.R.; Elechiguerra, J.L.; Camacho, A.; Holt, K.; Kouri, J.B.; Ramirez, J.T.; Yacaman, M.J. The bactericidal effect of silver nanoparticles. *Nanotechnology* **2005**, *16*, 2346–2353. [[CrossRef](#)]
9. Quinten, M.; Leitner, A.; Krenn, J.R.; Aussenegg, F.R. Electromagnetic energy transport via linear chains of silver nanoparticles. *Opt. Lett.* **1998**, *23*, 1331–1333. [[CrossRef](#)]
10. Nguyen, N.D.; Nguyen, T.V.; Chu, A.D.; Tran, H.V.; Tran, L.T.; Huynh, C.D. A label-free colorimetric sensor based on silver nanoparticles directed to hydrogen peroxide and glucose. *Arab. J. Chem.* **2018**, *11*, 1134–1143. [[CrossRef](#)]
11. Eising, R.; Elias, W.C.; Albuquerque, B.L.; Fort, S.; Domingos, J.B. Synthesis of silver glyconanoparticles from new sugar-based amphiphiles and their catalytic application. *Langmuir* **2014**, *30*, 6011–6020. [[CrossRef](#)]
12. Mallick, K.; Witcomb, M.; Scurrill, M. Silver nanoparticle catalysed redox reaction: An electron relay effect. *Mater. Chem. Phys.* **2006**, *97*, 283–287. [[CrossRef](#)]
13. Ren, X.; Meng, X.; Chen, D.; Tang, F.; Jiao, J. Using silver nanoparticle to enhance current response of biosensor. *Biosens Bioelectron* **2005**, *21*, 433–437. [[CrossRef](#)]
14. Arvizo, R.R.; Bhattacharyya, S.; Kudgus, R.A.; Giri, K.; Bhattacharya, R.; Mukherjee, P. Intrinsic therapeutic applications of noble metal nanoparticles: Past, present and future. *Chem. Soc. Rev.* **2012**, *41*, 2943–2970. [[CrossRef](#)]
15. Pugazhendhi, A.; Prabakar, D.; Jacob, J.M.; Karuppusamy, I.; Saratale, R.G. Synthesis and characterization of silver nanoparticles using *Gelidium amansii* and its antimicrobial property against various pathogenic bacteria. *Microb. Pathog.* **2018**, *114*, 41–45. [[CrossRef](#)]
16. Haes, A.J.; Duyne, R.P. Preliminary studies and potential applications of localized surface plasmon resonance spectroscopy in medical diagnostics. *Expert Rev. Mol. Diagn.* **2004**, *4*, 527–537. [[CrossRef](#)]
17. Raghavendra, G.M.; Jayaramudu, T.; Varaprasad, K.; Sadiku, R.; Ray, S.S.; Mohana Raju, K. Cellulose-polymer-Ag nanocomposite fibers for antibacterial fabrics/skin scaffolds. *Carbohydr. Polym.* **2013**, *93*, 553–560. [[CrossRef](#)]
18. Vu, X.H.; Duong, T.T.T.; Pham, T.T.H.; Trinh, D.K.; Nguyen, X.H.; Dang, V.-S. Synthesis and study of silver nanoparticles for antibacterial activity against *Escherichia coli* and *Staphylococcus aureus*. *Adv. Nat. Sci. Nanosci. Nanotechnol.* **2018**, *9*, 025019. [[CrossRef](#)]
19. Zhang, J.Z.; Noguez, C. Plasmonic Optical Properties and Applications of Metal Nanostructures. *Plasmonics* **2008**, *3*, 127–150. [[CrossRef](#)]
20. Zhang, M.L.; Fan, X.; Zhou, H.W.; Shao, M.W.; Zapien, J.A.; Wong, N.B.; Lee, S.T. A High-Efficiency Surface-Enhanced Raman Scattering Substrate Based on Silicon Nanowires Array Decorated with Silver Nanoparticles. *J. Phys. Chem. C* **2010**, *114*, 1969–1975. [[CrossRef](#)]
21. Ding, S.Y.; You, E.M.; Tian, Z.Q.; Moskovits, M. Electromagnetic theories of surface-enhanced Raman spectroscopy. *Chem. Soc. Rev.* **2017**, *46*, 4042–4076. [[CrossRef](#)] [[PubMed](#)]
22. Natsuki, J. A Review of Silver Nanoparticles: Synthesis Methods, Properties and Applications. *Int. J. Mater. Sci. Appl.* **2015**, *4*, 325–332. [[CrossRef](#)]
23. Abou El-Nour, K.M.M.; Eftaiha, A.a.; Al-Warthan, A.; Ammar, R.A.A. Synthesis and applications of silver nanoparticles. *Arab. J. Chem.* **2010**, *3*, 135–140. [[CrossRef](#)]
24. Jamkhande, P.G.; Ghule, N.W.; Bamer, A.H.; Kalaskar, M.G. Metal nanoparticles synthesis: An overview on methods of preparation, advantages and disadvantages, and applications. *J. Drug Deliv. Sci. Technol.* **2019**, *53*, 101174. [[CrossRef](#)]
25. Kibis, L.S.; Stadnichenko, A.I.; Pajetnov, E.M.; Koscheev, S.V.; Zaykovskii, V.I.; Boronin, A.I. The investigation of oxidized silver nanoparticles prepared by thermal evaporation and radio-frequency sputtering of metallic silver under oxygen. *Appl. Surf. Sci.* **2010**, *257*, 404–413. [[CrossRef](#)]
26. Dell’Aglia, M.; Mangini, V.; Valenza, G.; De Pascale, O.; De Stradis, A.; Natile, G.; Arnesano, F.; De Giacomo, A. Silver and gold nanoparticles produced by pulsed laser ablation in liquid to investigate their interaction with Ubiquitin. *Appl. Surf. Sci.* **2016**, *374*, 297–304. [[CrossRef](#)]

27. Jung, J.H.; Cheol Oh, H.; Soo Noh, H.; Ji, J.H.; Soo Kim, S. Metal nanoparticle generation using a small ceramic heater with a local heating area. *J. Aerosol Sci.* **2006**, *37*, 1662–1670. [[CrossRef](#)]
28. Li, J.; Zhu, J.; Liu, X. Ultrafine silver nanoparticles obtained from ethylene glycol at room temperature: Catalyzed by tungstate ions. *Dalton Trans.* **2014**, *43*, 132–137. [[CrossRef](#)]
29. Nasiriboroumand, M.; Montazer, M.; Barani, H. Preparation and characterization of biocompatible silver nanoparticles using pomegranate peel extract. *J. Photochem. Photobiol. B Biol.* **2018**, *179*, 98–104. [[CrossRef](#)]
30. Guzmán, M.G.; Dille, J.; Godet, S. Synthesis of silver nanoparticles by chemical reduction method and their antibacterial activity. *Int. J. Chem. Biomol. Eng.* **2009**, *2*, 104–111.
31. Toisawa, K.; Hayashi, Y.; Takizawa, H. Synthesis of Highly Concentrated Ag Nanoparticles in a Heterogeneous Solid-Liquid System under Ultrasonic Irradiation. *Mater. Trans.* **2010**, *51*, 1764–1768. [[CrossRef](#)]
32. Wagner, J.; Kohler, J.M. Continuous synthesis of gold nanoparticles in a microreactor. *Nano Lett.* **2005**, *5*, 685–691. [[CrossRef](#)]
33. Pryshchepa, O.; Pomastowski, P.; Buszewski, B. Silver nanoparticles: Synthesis, investigation techniques, and properties. *Adv. Colloid Interface Sci.* **2020**, *284*, 102246. [[CrossRef](#)]
34. Zhang, X.F.; Liu, Z.G.; Shen, W.; Gurunathan, S. Silver Nanoparticles: Synthesis, Characterization, Properties, Applications, and Therapeutic Approaches. *Int. J. Mol. Sci.* **2016**, *17*, 1534. [[CrossRef](#)]
35. Xu, P.F.; Liu, Z.H.; Duan, Y.H.; Sun, Q.; Wang, D.; Zeng, X.F.; Wang, J.X. Microfluidic controllable synthesis of monodispersed sulfur nanoparticles with enhanced antibacterial activities. *Chem. Eng. J.* **2020**, *398*, 125293. [[CrossRef](#)]
36. Luo, G.S.; Du, L.; Wang, Y.J.; Lu, Y.C.; Xu, J.H. Controllable preparation of particles with microfluidics. *Particuology* **2011**, *9*, 545–558. [[CrossRef](#)]
37. Jahn, A.; Reiner, J.E.; Vreeland, W.N.; DeVoe, D.L.; Locascio, L.E.; Gaitan, M. Preparation of nanoparticles by continuous-flow microfluidics. *J. Nanoparticle Res.* **2008**, *10*, 925–934. [[CrossRef](#)]
38. Shrimal, P.; Jadeja, G.; Patel, S. A review on novel methodologies for drug nanoparticle preparation: Microfluidic approach. *Chem. Eng. Res. Des.* **2020**, *153*, 728–756. [[CrossRef](#)]
39. Jiang, L.G.; Wang, W.P.; Chau, Y.; Yao, S.H. Controllable formation of aromatic nanoparticles in a three-dimensional hydrodynamic flow focusing microfluidic device. *Rsc Adv.* **2013**, *3*, 17762–17769. [[CrossRef](#)]
40. Lazarus, L.L.; Riche, C.T.; Marin, B.C.; Gupta, M.; Malmstadt, N.; Brutchey, R.L. Two-phase microfluidic droplet flows of ionic liquids for the synthesis of gold and silver nanoparticles. *ACS Appl. Mater. Interfaces* **2012**, *4*, 3077–3083. [[CrossRef](#)]
41. Lazarus, L.L.; Yang, A.S.; Chu, S.; Brutchey, R.L.; Malmstadt, N. Flow-focused synthesis of monodisperse gold nanoparticles using ionic liquids on a microfluidic platform. *Lab A Chip* **2010**, *10*, 3377–3379. [[CrossRef](#)] [[PubMed](#)]
42. Hartman, R.L.; McMullen, J.P.; Jensen, K.F. Deciding whether to go with the flow: Evaluating the merits of flow reactors for synthesis. *Angew. Chem. Int. Ed.* **2011**, *50*, 7502–7519. [[CrossRef](#)] [[PubMed](#)]
43. Song, H.; Chen, D.L.; Ismagilov, R.F. Reactions in droplets in microfluidic channels. *Angew. Chem. Int. Ed.* **2006**, *45*, 7336–7356. [[CrossRef](#)] [[PubMed](#)]
44. Li, L.L.; Li, X.D.; Wang, H. Microfluidic Synthesis of Nanomaterials for Biomedical Applications. *Small Methods* **2017**, *1*, 1700140. [[CrossRef](#)]
45. Brivio, M.; Verboom, W.; Reinhoudt, D.N. Miniaturized continuous flow reaction vessels: Influence on chemical reactions. *Lab A Chip* **2006**, *6*, 329–344. [[CrossRef](#)]
46. deMello, J.; deMello, A. Microscale reactors: Nanoscale products. *Lab Chip* **2004**, *4*, 11N–15N. [[CrossRef](#)]
47. Li, G.X.; Li, Q.; Cheng, R.; Chen, S. Synthesis of quantum dots based on microfluidic technology. *Curr. Opin. Chem. Eng.* **2020**, *29*, 34–41. [[CrossRef](#)]
48. Amreen, K.; Goel, S. Review-Miniaturized and Microfluidic Devices for Automated Nanoparticle Synthesis. *Ecs J. Solid State Sci. Technol.* **2021**, *10*, 017002. [[CrossRef](#)]
49. Zhang, M.J.; Wang, W.; Xie, R.; Ju, X.J.; Liu, Z.; Jiang, L.; Chen, Q.M.; Chu, L.Y. Controllable microfluidic strategies for fabricating microparticles using emulsions as templates. *Particuology* **2016**, *24*, 18–31. [[CrossRef](#)]
50. Chen, C.H.; Shah, R.K.; Abate, A.R.; Weitz, D.A. Janus particles templated from double emulsion droplets generated using microfluidics. *Langmuir* **2009**, *25*, 4320–4323. [[CrossRef](#)]
51. Shum, H.C.; Abate, A.R.; Lee, D.; Studart, A.R.; Wang, B.; Chen, C.H.; Thiele, J.; Shah, R.K.; Krummel, A.; Weitz, D.A. Droplet microfluidics for fabrication of non-spherical particles. *Macromol. Rapid Commun.* **2010**, *31*, 108–118. [[CrossRef](#)]
52. Wu, J.; Zhou, X.; Li, P.; Lin, X.; Wang, J.; Hu, Z.; Zhang, P.; Chen, D.; Cai, H.; Niessner, R.; et al. Ultrasensitive and Simultaneous SERS Detection of Multiplex MicroRNA Using Fractal Gold Nanotags for Early Diagnosis and Prognosis of Hepatocellular Carcinoma. *Anal. Chem.* **2021**, *93*, 8799–8809. [[CrossRef](#)]
53. Xu, L.; Peng, J.H.; Yan, M.; Zhang, D.; Shen, A.Q. Droplet synthesis of silver nanoparticles by a microfluidic device. *Chem. Eng. Process.-Process Intensif.* **2016**, *102*, 186–193. [[CrossRef](#)]
54. Magdalene, D.J.; Muthuselvam, D.; Pravinraj, T. Microfluidics-based green synthesis of silver nanoparticle from the aqueous leaf extract of *Ipomea quamoclit* L. *Appl. Nanosci.* **2021**, *11*, 2073–2084. [[CrossRef](#)]
55. Liu, G.J.; Ma, X.; Sun, X.D.; Jia, Y.H.; Wang, T.F. Controllable Synthesis of Silver Nanoparticles Using Three-Phase Flow Pulsating Mixing Microfluidic Chip. *Adv. Mater. Sci. Eng.* **2018**, *2018*, 3758161. [[CrossRef](#)]
56. Ryan, N.W.; Johnson, M.M. Transition from laminar to turbulent flow in pipes. *AIChE J.* **1959**, *5*, 433–435. [[CrossRef](#)]
57. Murphy, C.J. Materials science. Nanocubes and nanoboxes. *Science* **2002**, *298*, 2139–2141. [[CrossRef](#)]

58. Wang, W.; Efrima, S.; Regev, O. Directing Silver Nanoparticles into Colloid–Surfactant Lyotropic Lamellar Systems. *J. Phys. Chem. B* **1999**, *103*, 5613–5621. [[CrossRef](#)]
59. Foldbjerg, R.; Olesen, P.; Hougaard, M.; Dang, D.A.; Hoffmann, H.J.; Autrup, H. PVP-coated silver nanoparticles, and silver ions induce reactive oxygen species, apoptosis, and necrosis in THP-1 monocytes. *Toxicol. Lett.* **2009**, *190*, 156–162. [[CrossRef](#)]
60. Wang, M.; Li, H.; Li, Y.; Mo, F.; Li, Z.; Chai, R.; Wang, H. Dispersibility and Size Control of Silver Nanoparticles with Anti-Algal Potential Based on Coupling Effects of Polyvinylpyrrolidone and Sodium Tripolyphosphate. *Nanomaterials* **2020**, *10*, 1042. [[CrossRef](#)]
61. Munoz-Davila, M.J. Role of Old Antibiotics in the Era of Antibiotic Resistance. Highlighted Nitrofurantoin for the Treatment of Lower Urinary Tract Infections. *Antibiotics* **2014**, *3*, 39–48. [[CrossRef](#)] [[PubMed](#)]

Disclaimer/Publisher’s Note: The statements, opinions and data contained in all publications are solely those of the individual author(s) and contributor(s) and not of MDPI and/or the editor(s). MDPI and/or the editor(s) disclaim responsibility for any injury to people or property resulting from any ideas, methods, instructions or products referred to in the content.